2011-08-19

Guiding the experimental discovery of magnesium alloys

Richard H. Taylor

Gus L. W. Hart
gus.hart@gmail.com

Stefano Curtarolo

Original Publication Citation

Richard H. Taylor*, Stefano Curtarolo, Gus L. W. Hart, "Guiding the experimental discovery of novel magnesium alloys," Phys. Rev. B 84 8411 (211). The original article may be found here: http://prb.aps.org/abstract/PRB/v84/i8/e8411

Guiding the experimental discovery of magnesium alloys

Richard H. Taylor,[1,2] Stefano Curtarolo,[2,*] and Gus L. W. Hart[1,†]

[1]*Department of Physics and Astronomy, Brigham Young University, Provo, Utah 84602, USA*

[2]*Department of Mechanical Engineering and Materials Science and Department of Physics, Duke University, Durham, North Carolina 27708, USA*

(Received 4 February 2011; published 19 August 2011)

Magnesium alloys are among the lightest structural materials known and are of considerable technological interest. To develop superior magnesium alloys, experimentalists must have a thorough understanding of the concentration-dependent precipitates that form in a given system, and hence, the thermodynamic stability of crystal phases must be determined. This information is often lacking but can be supplied by first-principles methods. Within the high-throughput framework, AFLOW, $T = 0$ K ground-state predictions are made by scanning a large set of known candidate structures for thermodynamic (formation energy) minima. The following 34 systems are investigated: AlMg, AuMg, CaMg, CdMg, CuMg, FeMg*, GeMg, HgMg, IrMg, KMg*, LaMg, MgMo*, MgNa, MgNb*, MgOs*, MgPb, MgPd, MgPt, MgRb*, MgRe*, MgRh, MgRu, MgSc, MgSi, MgSn, MgSr, MgTa*, MgTc, MgTi*, MgV*, MgW*, MgY, MgZn, and MgZr (* = systems in which the *ab initio* method predicts that no compounds are stable). Avenues for further investigation are clearly revealed by this work. These include stable phases predicted in compound-forming systems as well as phases predicted in systems reported to be non-compound-forming.

DOI: 10.1103/PhysRevB.84.084101 PACS number(s): 61.50.Ah, 61.66.Dk, 81.30.Bx

I. INTRODUCTION

The importance of materials in modern society is difficult to overstate and continues to grow as twenty-first century challenges emerge. Concern over human energy consumption and environmental impact has become urgent in recent years, even making a striking entrance into the public discourse. Paralleling this, the desire for highly efficient materials tailored to specific applications has increased. A great deal of effort has focused on material weight and strength. Light, yet durable materials are needed in the automotive and aerospace industries, two sectors that are jointly responsible for a large source of anthropogenic pollutants and a significant portion of global energy consumption.[2]

Magnesium (Mg) alloys are among the lightest structural materials known and are used in a variety of applications, particularly in automotive and aerospace manufacturing. The abundance of magnesium is an important practical consideration and suggests that increased consumption could be sustained. Indeed, over the past decade Mg consumption has increased dramatically due in large part to an impetus in the automotive industry toward lighter, more energy efficient vehicles. This has been accompanied by an increase of Mg research, and although much progress has been made toward a complete understanding of Mg alloys, much remains to be done.

In improving or designing alloys, materials scientists rely on the thermodynamic information in published phase diagrams. This information is found directly through experimental reports and by modeled data (e.g., using the Calculation of Phase Diagrams (CALPHAD) method). However, thermodynamic data for even common alloys is sometimes incomplete. This is due, at least in part, to the difficulty of achieving thermodynamic equilibrium at low temperatures and the inability to make accurate models from incomplete or unreliable experimental data sets. First-principles (*ab initio*) methods provide a powerful tool in this arena and can be used to complete our understanding of the low-temperature thermodynamics of alloys.

Ab initio methods have long been recognized as a viable approach to the study of materials and have already been applied to a number of Mg systems (see, for example, Refs. 3 and 4). Accurate formation energy predictions at zero temperature only require details of the crystal structure and composition, and although calculations of this sort are slow compared to very fast models such as cluster expansion, they are not limited to derivative superstructures of a parent lattice. In a *high-throughput* (HT) approach, searches over many crystallographic types can be made, thereby introducing the possibility of making surprising (even off-lattice) predictions. Ground-state predictions made in this manner are typically in very good agreement with experimental results, as shown by Curtarolo, Morgan, and Ceder[5] in a review of 80 binary systems.

Using the HT framework AFLOW,[5–12] we have explored the full composition range of 34 Mg-X binary systems at $T = 0$ K. In the large majority of cases, our calculations are consistent with experimental phases. That is, the ordered phases shown in the phase diagram coincide with the low-temperature ground-state predictions of the HT approach. In nearly all the remaining cases, the differences between the HT results and phase diagrams are relatively minor (though the differences may still indicate opportunities for alloy design). Finally, there are some instances of strong disagreement, but they are few. Included in these are three non-compound-forming systems reported here with one or more stable *ab initio* compounds.

The remainder of the paper progresses as follows. After a discussion of the HT methodology and library, systems without *ab initio* compounds are reported. Following this, compound-forming systems are summarized and then discussed system by system. These are presented in alphabetical order with tables containing summarizing data related to each. Plots showing

formation energy versus atomic percent Mg for each system are also included.

II. METHOD

In the HT approach used here, the ground-state profile of a binary system is studied by a correlated brute force search. Formation energies (calculated with respect to the most stable structure of the pure elements) are obtained for all common prototypes for the class under investigation (i.e., Mg-X) as well as for a large number of enumerated derivative superstructures.[13] This procedure has given reasonable results for a large number of systems, as described in Ref. 5. Here it was shown that the probability of reproducing the correct ground state, if well defined, not ambiguous, and present in the list of prototypes, was $\eta_c^\star \sim 96.7\%$ (*"reliability of the method,"* Eq. (3) of Ref. 5).

The accuracy of the method can be quantified in a similar manner for the systems included in this paper. As an upper bound we may consider the correct ground state to be obtained when the experimental phase is predicted close to the energy of the tie line. In particular, accurate predictions will include lowest-energy phases at a given composition that are in agreement with the experimental phase but do not contribute to the convex hull topology (are slightly above the tie line) or are only a few meV above a related *ab initio* ground state. In the latter case, stabilization at finite temperature may be due to, for instance, vibrational entropy. Finally, in this estimation of the method's accuracy, only unambiguously defined phases present in the list of prototypes are considered as valid comparisons.

The total number of *potential structure comparisons* (i.e., all instances of experimentally determined intermetallic phases in the systems included in this study) is 58. Some of these were not available as comparison structures due to either ambiguity in the definition, unknown prototypes, or large unit cells. When these are excluded, we find the *total available structure comparisons* ($N_t = 45$). The available structure comparisons can be divided into those with *exact ab initio agreement* ($N_e = 38$), *possible or likely ab initio agreement* ($N_p = 7$) [small deviations from the convex hull energy likely due to (i) calculation error and/or (ii) entropic effects], and *clear disagreement* ($N_d = 1$).

Let the total number of non-compound-forming systems ($N_{ti} = 12$) be divided into *ab initio* agreements ($N_{ai} = 11$) and disagreements ($N_{di} = 1$). (The Mg-Zr and Mg-Tc systems are excluded due to a lack of reliable experimental data across the entire composition range.) A lower bound (LB) on the accuracy of our method in the Mg-X systems studied here is provided by the ratio of exact *ab initio* agreement to the number of available structure comparisons:

$$\eta_{\mathrm{LB}} = \frac{N_e + N_{ai}}{N_t + N_{ti}} \approx 86.0\%. \tag{1}$$

We find the upper bound (UB) on the reliability of our method by the ratio of correct compounds including possible and likely *ab initio* agreement and non-compound-forming systems ($N_e + N_p + N_{ai}$) to the total number of available structure and non-compound-forming system comparisons ($N_t + N_{ti}$):

$$\eta_{\mathrm{UB}} \equiv \frac{N_e + N_p + N_{ai}}{N_t + N_{ti}} \approx 98.2\%. \tag{2}$$

Therefore, the accuracy of the method (η_c) in reproducing the correct ground state of the included systems, if present in the list of prototypes and unambiguously defined, is estimated to be between $\eta_{\mathrm{LB}} \approx 86.0\%$ and $\eta_{\mathrm{UB}} \approx 98.2\%$:

$$86.0\% \leqslant \eta_c \leqslant 98.2\%. \tag{3}$$

Of course, there is no guarantee that the *true* ground states of a system will be found among the common experimentally observed structures or among small-unit-cell derivative structures. Nevertheless, even if it is impossible to rule out the existence of an alternate ground state, this procedure (searching many enumerated derivative structures and exploring common and related experimentally reported structures) is expected to give a reasonable balance between HT speed and scientific accuracy to determine the $T = 0$ K ground states of Mg-X systems.

Calculations were performed within the AFLOW framework with *ab initio* calculations of the energies given by the VASP software.[14] We mainly used projector augmented wave (PAW) pseudopotentials[15] and the exchange-correlation functionals parameterized by Perdew, Burke, and Ernzerhof (PBE)[16] for the generalized gradient approximation (GGA) (exceptions to this are described in the next section). The energies were calculated at zero temperature (K) and pressure, so that energies and enthalpies coincide, with spin polarization and without zero-point motion or lattice vibrations. Zero-point motion is negligible in this study because we do not consider alloys with the lightest elements (e.g., H, Li). All crystal structures were fully relaxed (cell volume and shape and atomic positions). Numerical convergence to about $\sim$1 meV/atom was ensured by a high-energy cutoff (30% higher than the highest energy cutoff for the pseudopotentials of the components) and dense 6000–8000 **k**-point Monkhorst-Pack meshes.

A. Structure library

The energies of around 250 crystal structures were calculated for each of the Mg-X systems studied. In addition to the 176 configurations described in Ref. 5, these included all the symmetrically distinct hcp-, bcc-, and fcc-based superstructures[13] with up to four atoms per cell and the prototypes A5, A6, A7, A8, A9, A11, A13, A12, B20, C1, C_b, C36, $D0_{19}$, $D0_{21}$, $D5_{19}$, $D8_c$, $D8_{11}$, $AuMg_2$, Al_2Zr_4, Al_3Zr_2, $Au_{3\pm x}Mg$, CdTi, $CuPt_7$, Cu_3Ti_2, Ga_2Hf, Ga_4Ni, Ga_3Pt_5, Ga_4Ti_5, Hg_2Pt, ITl, InTh, LiB-MS1/2 (Refs. 8,9,11,17 and 18), $Mg_{44}Rh_7$, $Mg_{38}Sr_9$, $Mn_{23}Th_6$, $NbNi_8(Pt_8Ti)$, $Ni_{17}Th_2$, $NiTi_2$, SeTl, and V_4Zn_5. The additional prototypes were considered because they are common or related to Mg alloys.[19,20] Crystallographic data for less familiar prototypes arising in our study (relaxed and unrelaxed) are given in Tables I, II, and III.

The solute elements considered in this study are the following: Al, Au, Ca, Cd, Cu, Fe, Ge, Hg, Ir, K, La, Mo, Na, Nb, Os, Pb, Pd, Pt, Rb, Re, Rh, Ru, Sc, Si, Sn, Sr, Ta, Tc, Ti, V, W, Y, Zn, and Zr. This includes most of the transition metals and several other alloys, including some with industrial importance (e.g., Al, Ca). Although also systems of interest, Ag-Mg, Hf-Mg, In-Mg, and Li-Mg were not included because one or more of the authors have already reported HT *ab initio* data on these systems.[5,9,10,21]

TABLE I. Crystallographic data for unrelaxed bcc-, fcc-, and hcp-derived prototypes arising in our study.

Compound	AB_4 (Ref. 1)	AB_3	A_2B_2	A_2B_2	A_2B_2	A_2B_2
Superlattice	fcc	bcc	bcc	bcc	fcc	fcc
Lattice	monoclinic	monoclinic	orthorhombic	orthorhombic	monoclinic	tetragonal
Space group	$C2/m$ 12	$P2/m$ 10	*Cmma* 67	*Imma* 74	$C2/m$ 12	$P4/nmm$ 129
Pearson symbol	mS10	mP4	oS8	oI8	mS8	tP4
Primitive vector						
a_1/a	(1/2,1/2,0)	(0,−2,0)	(1/2,1/2,1/2)	(3/2,1/2,−1/2)	(−1/2,1,−1/2)	(0,−1/2,−1/2)
a_2/a	(0,5/2,5/2)	(−1,0,−1)	(−1/2,−1/2,1/2)	(1/2,3/2,1/2)	(−1/2,1/2,−1)	(0,−1/2,1/2)
a_3/a	(1/2,1,3/2)	(1/2,5/2,−1/2)	(2,−2,0)	(−1/2,−3/2,1/2)	(0,−2,2)	(−2,0,0)
Atomic positions						
A1	(0,0,0)	(0,0,0)	(0,0,0)	(0,0,0)	(0,0,0)	(0,0,0)
A2	–	–	(1/2,1/2,3/4)	(1/4,3/4,1/2)	(0,0,3/4)	(1/2,1/2,3/2)
B1	(0,1/5,0)	(3/4,1/2,0)	(0,0,1/2)	(1/2,1/2,0)	(0,0,1/4)	(0,0,1/2)
B2	(0,2/5,0)	(1/2,0,0)	(1/2,1/2,1/4)	(3/4,1/4,1/2)	(0,0,1/2)	(1/2,1/2,1/4)
B3	(0,3/5,0)	(1/4,1/2,0)	–	–	–	–
B4	(0,4/5,0)	–	–	–	–	–
AFLOW label	"f52"	"73/75"	"71"	"80"	"17"	"14"

In the systems Al-, Ge-, and Si-Mg, anomalously low energies (many meV below the next lowest energies) were obtained for the Be_2Zn structure. The topology of the convex hull was in these instances entirely determined by the Be_2Zn phase. This led to results in complete contradiction of experiment. Furthermore, the relaxed atomic volumes were found to be inexplicably lower than the constituent element values and neighboring structures. For the Al-, Ge-, and Si-Mg systems, the combination of PBE functionals and VASP apparently led to the erroneous results. When the local density approximation (LDA) or Perdew and Wang[22] (PW) functionals were used, reasonable results were obtained. These were further corroborated by linearized augmented plane-wave (LAPW) calculations using the WIEN2K package.[23] In these three cases, the Be_2Zn structure had positive formation energy and reasonable equilibrium atomic volumes. Experimental ground states were also largely confirmed. Therefore, the results reported in this paper for Al-, Ge-, and Si-Mg are based on PW functionals. Further discussion of the unusual behavior exhibited when the PBE parametrization is used is beyond the scope of this paper.

TABLE II. Crystallographic information for less familiar prototypes arising in our study. Atomic positions and unit cell parameters are fully relaxed [indicated by a star (⋆)]. Corresponding unrelaxed structures are given in Table III.

Compound	Be_2Zn-65⋆ (Ref. 12)	Hf_5Pb-f63⋆ (Ref. 9)	Hf_2Tl-6⋆ (Ref. 9)
Lattice	orthorhombic	tetragonal	tetragonal
Space group	*Fmmm* 69	$P4/mmm$ 123	$I4/mmm$ 139
Pearson symbol	oF12	tP6	tI6
Primitive vector	(SG option 2)	–	(SG option 2)
(a,b,c) (Å)	(3.780, 2.0978, 10.3)	(3.203,3.203,13.944)	(4.422,4.422,7.385)
(α,β,γ) (deg)	(90,90,90)	(90,90,90)	(90,72.577,90)
Wyckoff	(0,0,0.17832) 8i Be1	(0,0,−0.1794) 2g Hf1	(0,0,0.1746) 4e Hf1
positions	(0,0,1/2) 4b Zn1	(1/2,1/2,−0.3349) 2h Hf2	(0,0,1/2) 2b Tl2
	–	(0,0,1/2) 1b Hf3	–
	–	(1/2,1/2,0) 1c Pb1	–
AFLOW label	"549"	"477"	"547"
Compound	Mo_3Ti-81⋆ (Ref. 12)	$HfPd_5$-f137⋆ (Ref. 9)	Re_3Ru-124⋆ (Ref. 12)
Lattice	orthorhombic	orthorhombic	orthorhombic
Space group	*Immm* 71	*Cmmm* 65	$Imm2$ 44
Pearson symbol	oI8	oS12	oI8
Primitive vector	(4.444,3.173,8.971)	(11.998,4.0663,14.0723)	(9.005,2.757,4.775)
	(90,90,90)	(90,90,90)	(90,90,90)
Wyckoff	(0,0,0.2440) 4i Mo1	(0,0,0) 2a Hf1	(1/4,0,0) 4c Re1
positions	(0,1/2,0) 2d Mo2	(0.1663,0,1/2) 4h Pd1	(0,1/2,1/6) 2b Re2
	(1/2,0,0) 2b Ti1	(0.3369,0,0) 4g Pd2	(0,0,2/3) 2a Ru1
	–	(1/2,0,1/2) 2c Pd3	–
AFLOW label	"541"	"479"	"551"

TABLE III. Crystallographic data for unrelaxed prototypes reported in Table II.

Compound	Be_2Zn (Ref. 12)	Hf_5Pb (Ref. 9)	Hf_2Tl (Ref. 9)	Re_3Ru (Ref. 12)	Mo_3Ti (Ref. 12)	$HfPd_5$ (Ref. 9)
Superlattice	bcc	fcc	fcc	hcp	bcc	hcp
Lattice	orthorhombic	tetragonal	tetragonal	orthorhombic	orthorhombic	orthorhombic
Space group	*Fmmm* 69	$P4/mmm$ 123	$I4/mmm$ 139	$Imm2$ 44	*Immm* 71	*Cmmm* 65
Pearson symbol	oF12	tP6	tI6	oI8	oI8	oS12
Primitive vector						
a_1 /a	(0,1,2)	(1/2,1/2,0)	(3/2,0,−1/2)	$(1/2,-\sqrt{2}/3,1.633)$	(3/2,1/2,−1/2)	(1/2,3/2,1)
a_2/a	(−1/2,3/2,3/2)	(0,3,3)	(3/2,0,1/2)	$(-1/2,\sqrt{2}/3,1.633)$	(1/2,3/2,1/2)	(0,3,3)
a_3/a	(−1/2,−1/2,1/2)	(1/2,5/2,3)	(−3/2,−1/2,0)	$(-1/2,-\sqrt{2}/3,-1.633)$	(−1/2,−3/2,1/2)	(1/2,3/2,2)
Atomic positions						
A1	(0,0,0)	(0,0,0)	(2/3,2/3,0)	(0,0,0)	(0,0,0)	(0,1/6,0)
A2	(2/3,2/3,1/3)	(0,1/6,0)	(1/3,1/3,0)	(1/2,1/2,0)	(1/4,3/4,1/2)	(0,1/3,0)
A3	–	(0,1/3,0)	–	(1/12,3/4,1/3)	(1/2,1/2,0)	(0,1/2,0)
A4	–	(0,1/2,0)	–	–	–	(0,2/3,0)
A5	–	(0,2/3,0)	–	–	–	(0,5/6,0)
B1	(1/3,1/3,2/3)	(0,5/6,0)	(0,0,0)	(7/12,1/4,1/3)	(3/4,1/4,1/2)	(0,0,0)
AFLOW label	"65"	"f63"	"6"	"124"	"81"	"f137"

III. RESULTS AND DISCUSSION

A. Non-compound-forming systems

No stable compounds were found in the following immiscible systems: Fe-Mg, K-Mg, Mg-Mo, Mg-Nb, Mg-Os, Mg-Rb, Mg-Re, Mg-Ta, Mg-Ti, Mg-V, and Mg-W. Non-compound-forming systems predicted by our study (identified by a complete lack of phases with negative formation energies) were in every case also reported to be without intermediate phases experimentally. The converse, however, was not always true. Several systems reported to be non-compound-forming produced thermodynamically stable compounds. These systems, Na-, Tc-, and Zr-Mg, are included in what follows (see also Table IV). This ostensible disagreement with experiment is not altogether surprising; Na is reactive, and experimental data for the Mg-Tc and Mg-Zr systems are incomplete.

B. Systems with *ab initio* compounds

All low-temperature experimental and $T = 0$ K *ab initio* ground states are described by individual system tables (a summary of *ab initio*–experimental disagreement is given in Table V). In the system tables (Tables VI–XXVIII), compounds are reported in order of increasing Mg content, with Mg concentration given in the first column, experimental results given in the second column, and *ab initio* results given in the third column. Relative formation energies may be given in instances of (a) very close (in energy) competing phases, (b) when experimental phases are many meV/atom above the *ab initio* ground state, or (c) when an *ab initio* ground state does not exist. In non-compound-forming systems with *ab initio* ground states, the formation energy is given. In systems without known phase diagrams, experimental results are indicated by a dash (—) when compared to *ab initio* results. Experimental phases with unit cells too large to be accurately studied by HT *ab initio* methods are indicated by three stars (***). If the experimental compound is undetermined, this is denoted by *unknown*. Structures marked with an asterisk (e.g., A_2B^*-65) are relaxed prototypes and are described in the Tables I, II, and III. If necessary, Pearson symbols and space group number are listed in parentheses.

TABLE IV. Non-compound-forming systems with *ab initio* compounds. The enthalpy of the *ab initio* ground state (first and second columns) is reported in the third column.

System	Composition	Compound	Enthalpy (meV/atom)
Mg-Na	Mg_3Na_2	Al_3Zr_2	−223.9
Mg-Tc	$MgTc_2$	$C11_b$	−15.8
	Mg_3Tc_4	Cu_4Ti_3	−20.2
	MgTc	B11	−22.4
Mg-Zr	Mg_3Zr_4	Cu_4Ti_3	−31.6
	MgZr	B11	−31.3

1. Al-Mg (aluminum-magnesium)

No simple experimental compounds exist in the Al-Mg system. Two complex low-temperature phases are reported in

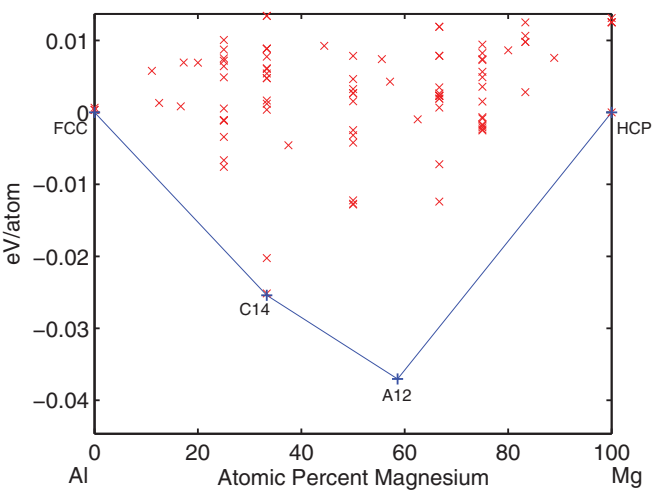

FIG. 1. (Color online) Al-Mg convex hull.

TABLE V. Summary of *ab initio*–experimental disagreements. A dash (—) indicates a system without an assessed phase diagram. Details are as follows: (a) discrepancy due to limited experimental data or system believed to be non-compound-forming, (b) structural properties of experimental compound are not fully known, (c) *ab initio* formation energy lower or higher than experimental phase energy alters tie line, and (d) experimental phase not (or only roughly) evaluated due to large cell size or partial occupation.

System	Composition	Experimental results	*Ab initio* result	Details
Al-Mg	Al_2Mg	two-phase region	C14/C36	(a)
Au-Mg	Au_5Mg	solid solution	$HfPd_5$	(a)
	Au_3Mg_5	two-phase region	$D8_m$	(a)
Cd-Mg	$CdMg_2$	two-phase region	$InMg_2$	(c)
Hg-Mg	Hg_2Mg	$C11_b$	C_c	(c)
	Hg_2Mg_5	Hg_2Mg_5 *unknown*	two-phase region	(b)
	$HgMg_3$	$D0_{18}$	two-phase region	(c)
Ir-Mg	Ir_7Mg	–	Ca_7Ge	(a)
	Ir_3Mg	–	$Re_3Ru^{\star}$-124	(a)
	IrMg	–	$FCC^{[311]}_{A2B2}$	(a)
	$IrMg_4$	$IrMg_4$ *unknown*	two-phase region	(b)
La-Mg	La_7Mg	two-phase region	Ca_7Ge	(a)
	$LaMg_{12}$	$LaMg_{12}$ *unknown*	two-phase region	(a)
Mg-Na	Mg_3Na_2	non-compound-forming	Al_3Zr_2	(a)
Mg-Pb	$MgPb_3$	two-phase region	AB_3-75	(a)
	MgPb	two-phase region	$L1_1$	(a)
Mg-Pd	$MgPd_7$	two-phase region	Ca_7Ge	(a)
	$MgPd_4$	two-phase region	$D1_a$	(a)
	$MgPd_3$	two-phase region	$D0_{23}$	(a)
	$MgPd_2$	two-phase region	C37	(a)
	Mg_3Pd_5	two-phase region	Ga_3Pt_5	(a)
	Mg_2Pd	two-phase region	$NiTi_2$/C16	(c)
	Mg_3Pd	$D0_{18}$	$D0_{21}$	(c)
	Mg_4Pd	Mg_4Pd *unknown*	two-phase region	(b)
	$\sim Mg_6Pd$	$Mg_{85}Pd_{14}$ *unknown*	two-phase region	(d)
Mg-Pt	$MgPt_7$	$MgPt_7$ *unknown*	Ca_7Ge	(b)
	$MgPt_2$	–	Ga_2Hf	(a)/(c)
	MgPt	FeSi-B20	$L1_0$	(d)
	Mg_2Pt	–	C16	(a)/(c)
Mg-Rh	$MgRh_7$	–	Ca_7Ge	(a)/(c)
	$MgRh_3$	–	$Re_3Ru^{\star}$-124	(a)/(c)
	Mg_2Rh	–	$Hf_2Tl^{\star}$-6	(a)/(c)
	Mg_3Rh	–	$D0_{21}$	(a)/(c)
Mg-Ru	$Mg_{44}Rh_7$	$Mg_{44}Rh_7$	two-phase region	(b)/(d)
Mg-Sc	$MgSc_2$	two-phase region	C49	(a)
	Mg_3Sc	two-phase region	$D0_{19}/L1_2$	(a)
Mg-Sr	$Mg_{38}Sr_9$	$Mg_{38}Sr_9$	two-phase region	(a)/(d)
Mg-Tc	$MgTc_2$	non-compound-forming	$C11_b$	(a)
	Mg_3Tc_4	non-compound-forming	Cu_4Ti_3	(a)
	MgTc	non-compound-forming	B11	(a)
Mg-Y	MgY_2	two-phase region	C49	(c)
	Mg_3Y	two-phase region	$D0_3/D0_{19}$	(c)
	$Mg_{24}Y_5$	A12	two-phase region	(c)/(d)
Mg-Zn	Mg_4Zn_7	Mg_4Zn_7	two-phase region	(c)/(d)
	MgZn	unknown	two-phase region	(b)
	Mg_2Zn	two-phase region	C16	(a)
Mg-Zr	Mg_3Zr_4	non-compound-forming	Cu_4Ti_3	(a)
	MgZr	non-compound-forming	B11	(a)

experimental phase diagrams: $Al_{12}Mg_{17}$-A12 and $Al_{45}Mg_{28}$-β. We did not calculate formation energy for the β structure due to the large unit cell and partial occupation of sites. Thus, although a stable phase is predicted by *ab initio* calculations at composition Al_2Mg, the system must be investigated further to more accurately predict phase(s) at Mg concentration less than $\sim$50%. It is known that the β phase undergoes a Martensitic transformation to another structure (possibly a distortion of β)

TABLE VI. The Al-Mg system.

Comparison of low temperature phases		
Composition % Mg	Experimental results[20,24–47]	*Ab initio* results (Fig. 1)
33.3	*two-phase region*	Ag_2Mg-C14/C36 C15 $\sim$ 5.20 meV/atom *above* C14
$\sim$38.4	$Al_{45}Mg_{28}$	***
$\sim$58.6	$Al_{12}Mg_{17}$-A12	A12

at low temperature.[20] In agreement with experiment, the A12 phase is a thermodynamic minimum.

2. Au-Mg (gold-magnesium)

The Au-Mg phase diagram is incomplete, particularly on the Au-rich side. An *ab initio* phase is predicted in this region with the $HfPd_5$ structure reported in Ref. 9. We evaluated the off-stoichiometry orthorhombic phases, $AuMg_{3-x}$ (oS160, 63) and $AuMg_{3+x}$ (oS64, 63), and the $D0_{23}$ phase at composition Au_3Mg. The orthorhombic phase formation energies differ by less than 1 meV, within numerical error, and are thus both reported as the ground state. The phase with structure $D0_{23}$ is a few meV above the stable compounds $AuMg_{3-x}$ and $AuMg_{3+x}$. Indeed, $D0_{23}$ is not expected to be stable at T = 0 K: experiment reports the phase only forming above $\sim$645 °C.[20]

On the Mg-rich side, the experimental phases AuMg-B2, $AuMg_2$ (oP108, 62), and $AuMg_{2.82}$-$D0_{21}$ are stable. An additional *ab initio* phase with the Au_3Mg_5-$D8_m$ structure is also stable.

TABLE VII. The Au-Mg system

Comparison of low temperature phases		
Composition % Mg	Experimental results[20,48–50]	*Ab initio* results (Fig. 2)
16.6	*solid solution*	$HfPd_5$[9]
25.0	$Au_{3-x}Mg/Au_{3+x}Mg$ Au_3Mg-$D0_{23}$ *high-temperature*	$Au_{3-x}Mg/Au_{3+x}Mg$ $D0_{23}$ $\sim$ 3.4 meV/atom *above* $Au_{3-x}Mg$
50.0	AuMg-B2	$B2/L1_0$
62.5	*two-phase region*	Au_3Mg_5-$D8_m$
66.6	$AuMg_2$	$AuMg_2$
$\sim$75.0	$AuMg_3$-$D0_{21}$	$D0_{21}$

3. Ca-Mg (calcium-magnesium)

Ca-Mg is a simple eutectic system having one intermetallic compound. The experimental phase forms at composition $CaMg_2$ with the C14 Laves structure. Experimental phase diagrams show the phase melts congruently with no homogeneity field. *Ab initio* calculations reveal a single ground state at the same composition with the C14 structure. The two additional Laves phase polytypes C36 and C15 are close in formation energy. The close structural similarity between these close-in-energy phases suggests dominant short-range interactions.

TABLE VIII. The Ca-Mg system.

Comparison of low temperature phases		
Composition % Mg	Experimental results[20,51–57]	*Ab initio* results (Fig. 3)
66.6	$CaMg_2$-C14	C14 C36 $\sim$ 2.3 meV/atom C15 $\sim$ 4.2 meV/atom *above* C14

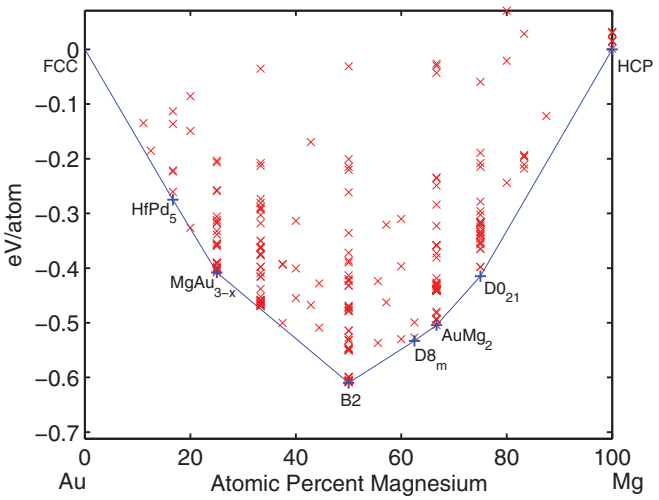

FIG. 2. (Color online) Au-Mg convex hull.

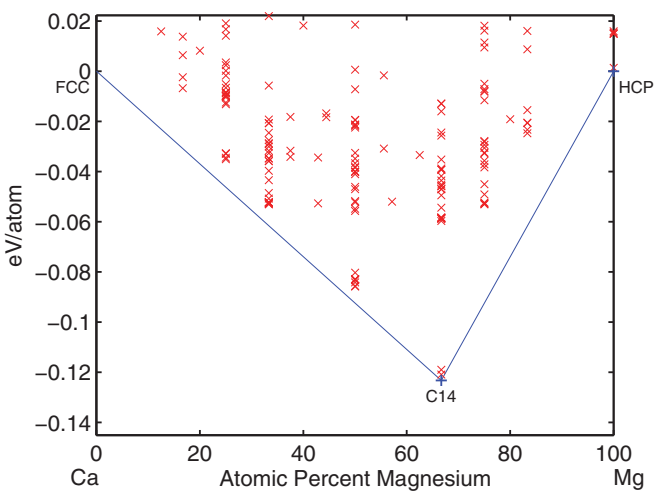

FIG. 3. (Color online) Ca-Mg convex hull.

4. Cd-Mg (cadmium-magnesium)

Experimental phase diagrams indicate intermetallic compounds with structures Cd_3Mg-$D0_{19}$, CdMg-B19, and $CdMg_3$-$D0_{19}$. *Ab initio* ground states exist at the same compositions with identical structures. An additional phase is predicted at composition $CdMg_2$ with the $InMg_2$ structure.

TABLE IX. The Cd-Mg system.

Comparison of low temperature phases		
Composition % Mg	Experimental results[20,58–73]	*Ab initio* results (Fig. 4)
∼25.0–32.0	Cd_3Mg-$D0_{19}$	$D0_{19}$
∼38.0–60.0	AuCd-B19	B19
66.6	*two-phase region*	$InMg_2$
∼65.0–82.0	$CdMg_3$-$D0_{19}$	$D0_{19}$

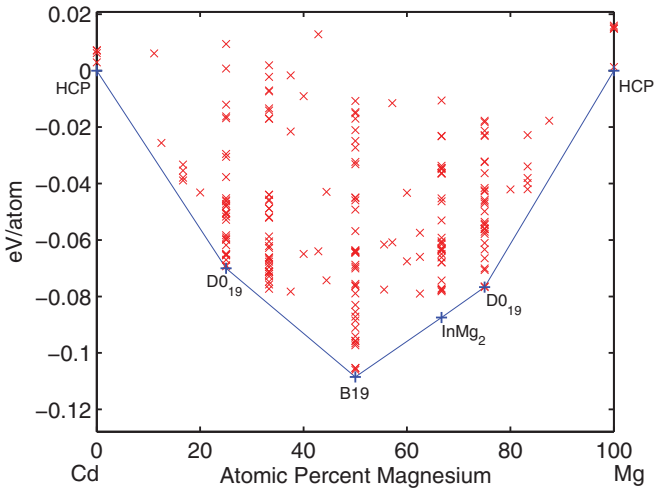

FIG. 4. (Color online) Cd-Mg convex hull.

5. Cu-Mg (copper-magnesium)

Ab initio ground states in the Cu-Mg system agree with experiment. Experimental phase diagrams show intermetallic compounds at compositions Cu_2Mg and $CuMg_2$ with the C15 and C_b structures, respectively. According to *ab initio* calculations, the Cu_2Mg-C15 structure is close in energy to the two other Laves phase polytypes, C36 and C14, suggesting weak long-range interactions.

TABLE X. The Cu-Mg system.

Comparison of low temperature phases		
Composition % Mg	Experimental results[20,74–78]	*Ab initio* results (Fig. 5)
∼31–35.3	Cu_2Mg-C15	C15 C36 ∼ 0.9 meV/atom C14 ∼ 2.1 meV/atom *above* C15
66.6	$CuMg_2$-C_b	C_b

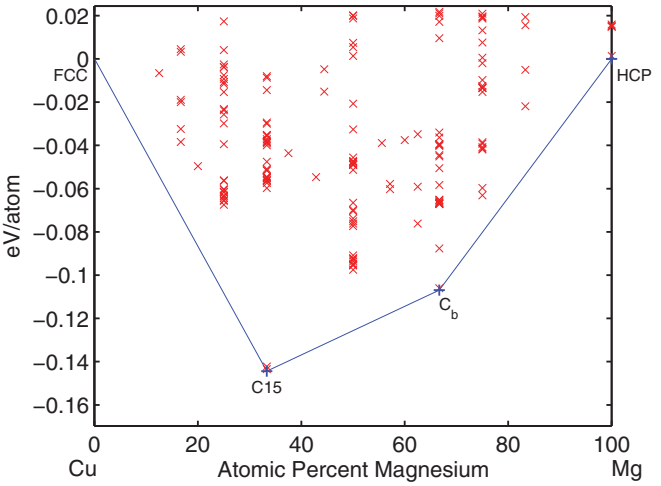

FIG. 5. (Color online) Cu-Mg convex hull.

Experimental phase diagrams show the phases melt congruently. Thus, given the agreement of the T = 0 K *ab initio* predictions, the phases may be stable from T = 0 K to the liquidus line.

6. Ge-Mg (germanium-magnesium)

A single *ab initio* compound is predicted to be thermodynamically stable in the Ge-Mg system. The phase, Ge_2Mg-C1, is in agreement with experimental data.

TABLE XI. The Ge-Mg system.

Comparison of low temperature phases		
Composition % Mg	Experimental results[20,79–82]	*Ab initio* results (Fig. 6)
66.6	Ge_2Mg-C1	C1

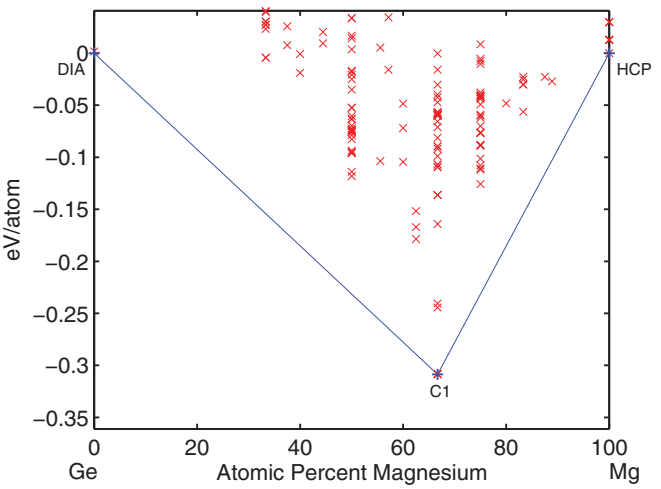

FIG. 6. (Color online) Ge-Mg convex hull.

7. *Hg-Mg (mercury-magnesium)*

Experimental phases are verified by *ab initio* calculations with differences at compositions Hg_2Mg and $HgMg_3$. The unidentified phase at composition Hg_2Mg_5 was not supported by *ab initio* results (no stable compound was found at this composition). However, this result is inconclusive, as only a small number of structures with the appropriate composition exist in the database.

The phases at compositions Hg_2Mg and $HgMg_3$ are not thermodynamically stable at $T = 0$ K, according to *ab initio* data, although phases with different structures are predicted relatively close to the tie line. The Hg_2Mg-C_c and $HgMg_3$-$D0_{19}$ phases are predicted instead of $C11_b$ and $D0_{19}$, respectively.

TABLE XII. The Hg-Mg system.

Comparison of low temperature phases		
Composition % Mg	Experimental results[20,83–85]	*Ab initio* results (Fig. 7)
33.3	Hg_2Mg-$C11_b$	*two-phase region* $C_c \sim 2.0$ meV/atom *above tie line* C37 ~ 21.4 meV/atom $C11_b \sim 22.0$ meV/atom *above* C_c
50.0	HgMg-B2	B2
62.5	Hg_3Mg_5-$D8_8$	$D8_8$
66.6	$HgMg_2$-C37	C37
71.4	Hg_2Mg_5 *unknown*	*two-phase region*
75.0	$HgMg_3$-$D0_{18}$	*two-phase region* $D0_{19} \sim 3.8$ meV/atom *above tie line* $D0_{18} \sim 28.5$ meV/atom *above* $D0_{19}$

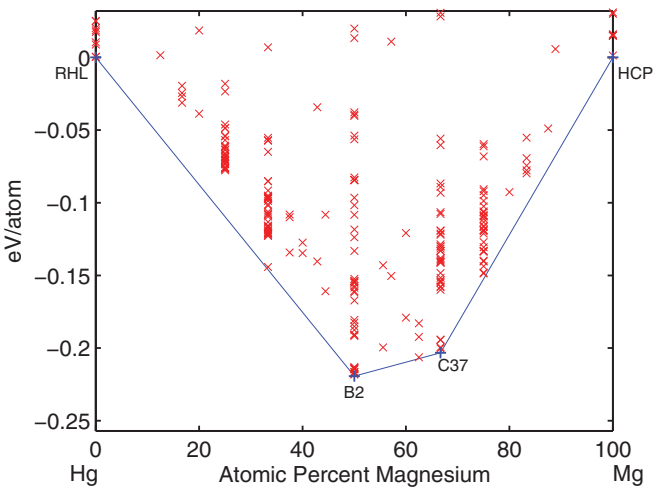

FIG. 7. (Color online) Hg-Mg convex hull.

8. *Ir-Mg (iridium-magnesium)*

Although Ir is rare and costly, it has remarkable physical and chemical properties.[86] Yet the very same properties that make it a material of interest (high melting point, resistance to corrosion, etc.) make the study of its alloys challenging.

TABLE XIII. The Ir-Mg system. A dagger (†) means see Tables II and III for crystallographic description.

Comparison of low temperature phases		
Composition % Mg	Experimental results[20,87]	*Ab initio* results (Fig. 8)
12.5	–	Ca_7Ge
25.0	–	$Re_3Ru^{\star}$-124†
		Ir_3Mg-"$L1_3$"[5] ~ 62.3 meV/atom
		above $Re_3Ru^{\star}$-124
50.0	–	$FCC^{[311]}_{A2B2}$
75.0	$IrMg_3$-$D0_{21}$	$D0_{21}$
80.0	$IrMg_4$ *unknown*	*two-phase region*
		$D1_a \sim 65.0$ meV/atom
		above tie line.
86.2	Ir_7Mg_{44}	$Ir_7Mg_{44} \sim 40.0$ meV/atom
		above tie line

Ir-Mg is no exception, and the experimental phase diagram for this system is not complete. Data are especially sparse at low temperatures, perhaps due to the high melting temperature of Ir. Experimental Ir-rich phases are unknown; the most Ir-rich phase is found at composition $IrMg_3$ with the $D0_{21}$ structure.

Given the lack of experimental data on the Ir-rich side, *ab initio* predictions are particularly interesting. Two *ab initio* Ir-rich phases are found: the fcc-derived Ca_7Ge structure and an hcp-derived prototype,[12] $Re_3Ru^{\star}$-124 described in Table II. An fcc-derived structure with A_2B_2 stacking along the [311] direction is thermodynamically stable at composition IrMg.

We are able to report with less certainty the Mg-rich phases. The experimental phase $Mg_{44}Ir_7$ (cF408, 216) was only roughly evaluated because of the large unit cell size. The **k**-point mesh was coarse by necessity, and it is likely the cell was not able to reach equilibrium volume. Nevertheless, the energy was found to be negative (∼40 meV above the tie line). The structural details of the reported phase at composition

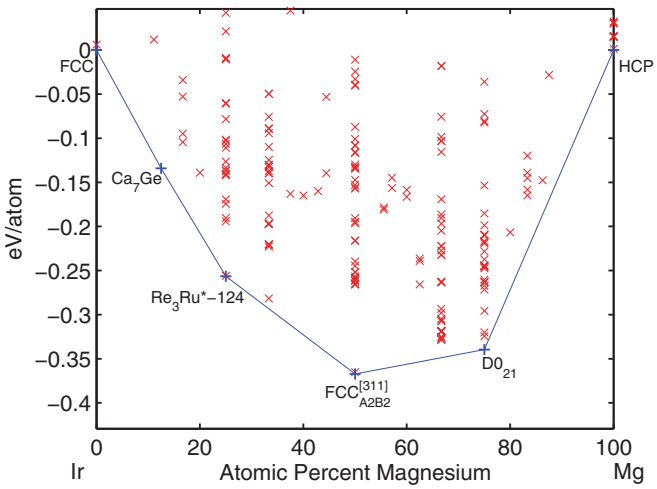

FIG. 8. (Color online) Ir-Mg convex hull.

$IrMg_4$ are not known, and thus the absence of a stable *ab initio* phase at this composition is indeterminate. Finally, the stability of the $IrMg_{2.82}$-$D0_{21}$ phase by *ab initio* calculations confirms experiment.

9. La-Mg (lanthanum-magnesium)

Stable *ab initio* phases agree with the La-Mg experimental phases LaMg-B2, $LaMg_3$-$D0_3$, and $Ni_{17}Th_2$. The structural data for the experimental phase at composition $LaMg_{12}$ is not complete, although a phase with a $CeMg_{12}$(II)-type structure has been proposed.[20] *Ab initio* calculations were not performed in this case due to the large unit cell size. La-rich phases have not been observed experimentally; however, an *ab initio* phase was predicted at composition La_7Mg with the Ca_7Ge structure.

TABLE XIV. The La-Mg System.

Comparison of low temperature phases		
Composition % Mg	Experimental results[20,88–93]	*Ab initio* results (Fig. 9)
12.5	*two-phase region*	Ca_7Ge
50.0	LaMg-B2	B2 NiTi ∼ 4.4 meV/atom *above* B2
75.0	$LaMg_3$-$D0_3$	$D0_3$ $D0_{19}$ ∼ 42.3 meV/atom *above* $D0_3$.
∼89.5	$Ni_{17}Th_2$	$Ni_{17}Th_2$
∼91.67–92.86	$LaMg_{12}$ *unknown/ CeMg*$_{12}$*(II)*	*two-phase region* ***

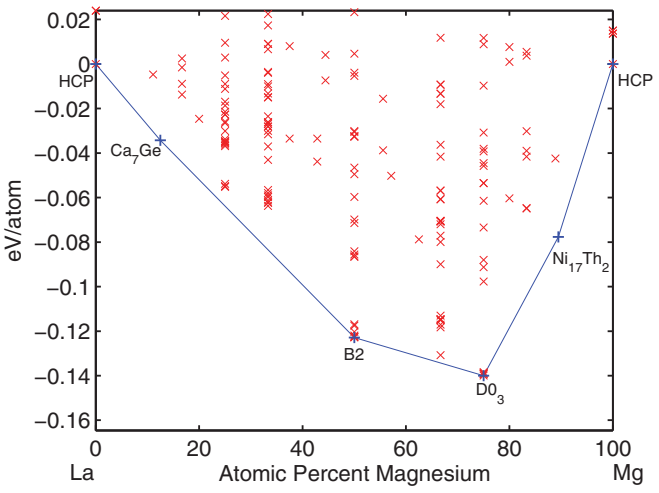

FIG. 9. (Color online) La-Mg convex hull.

10. Mg-Na (magnesium-sodium)

No intermetallic phases have been found in the Mg-Na system by experimental investigation.[20] An *ab initio* ground state is predicted at composition Mg_3Na_5 with the Al_3Zr_2-type structure (oF40, 43). Additional compounds with negative formation energies are found at compositions $MgNa_3$, Mg_2Na_3, Mg_3Na_2 with structures $FCC^{[111]}_{AB3}$ (4 atom unit cell, fcc-derived supercell with stacking along [111]), and Mg_3Na_2-C33.

TABLE XV. The Mg-Na system.

Comparison of low temperature phases		
Composition % Mg	Experimental results[20]	*Ab initio* results (Fig. 10)
60.0	*non-compound-forming*	Al_3Zr_2 ∼ -223.9 meV/atom C33 ∼ 199.5 meV/atom *above* Al_3Zr_2

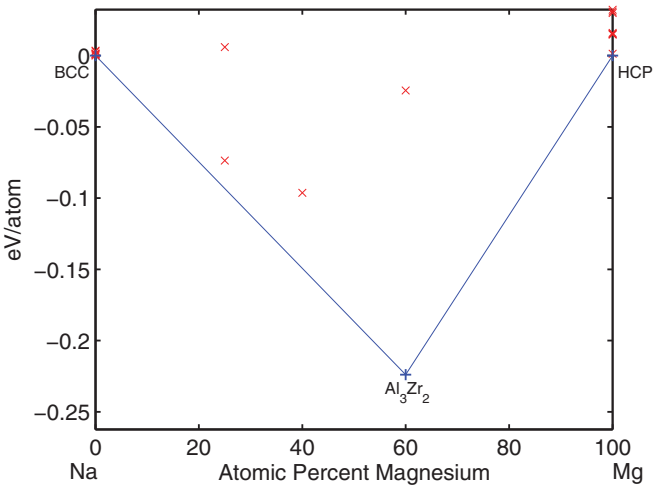

FIG. 10. (Color online) Mg-Na convex hull.

11. Mg-Pb (magnesium-lead)

Experimental phase diagrams indicate a single intermetallic compound at composition Mg_2Pb with the fluorite structure, C1. *Ab initio* calculations reveal additional phases $MgPb_3$-75 (see Table I for description), MgPb-$L1_1$, and Mg_3Pb-$L1_2$. A metastable phase with the $L1_2$ structure has been observed by splat cooling;[94] however, the phase decomposed into Mg(hcp) + Mg_2Pb-C1 when kept at room temperature. The stability of $L1_2$ at $T = 0$ K predicted by *ab initio* calculations suggests the phase may be stable at below room temperature.

TABLE XVI. The Mg-Pb System. A dagger (†) means see Tables I, II, and III for crystallographic description.

Comparison of low temperature phases		
Composition % Mg	Experimental results[20,95–102]	*Ab initio* results (Fig. 11)
25.0	*two-phase region*	AB_3-75†
50.0	*two-phase region*	MgPb-$L1_1$
66.6	Mg_2Pb-C1	C1
∼77.0–84.0	Mg_3Pb-$L1_2$ *(metastable)*	$L1_2$ Co_3V (hP24 *phase*) ∼2.4 meV/atom *above* $L1_2$

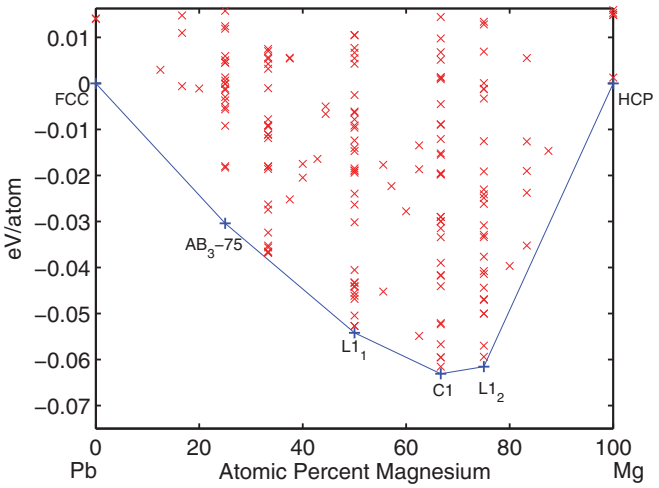

FIG. 11. (Color online) Mg-Pb convex hull.

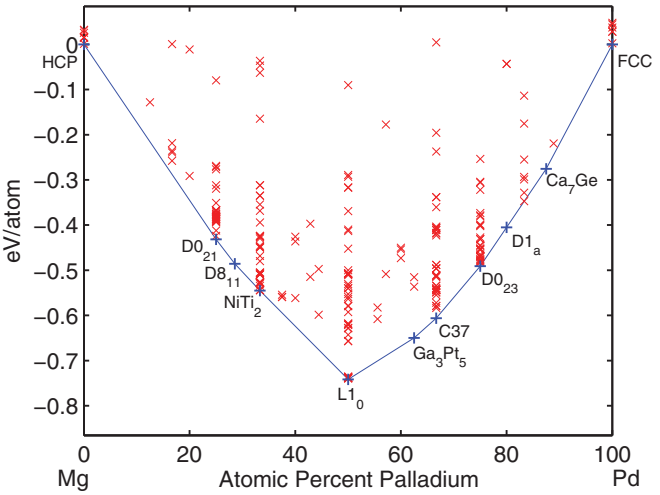

FIG. 12. (Color online) Mg-Pd convex hull.

12. Mg-Pd (magnesium-palladium)

Pd-rich compounds have not been identified in the Mg-Pd system. Five Pd-rich *ab initio* compounds are predicted, however: $MgPd_7$-Ca_7Ge, $MgPd_4$-$D1_a$, $MgPd_3$-$D0_{23}$, $MgPd_2$-C37, and Mg_3Pd_5-Ga_3Pt_5.

Two experimental phases have been identified near composition MgPd: $L1_0$ forms slightly off stoichiometry at composition $Mg_{0.9}Pd_{1.1}$ and is the only intermediate phase to melt congruently. The B2 phase forms as MgPd and undergoes a peritectic decomposition at ∼700 °C. The *ab initio* formation energies of these phases suggest that the $L1_0$ phase is the low-temperature ground state, although the difference in energy is not considerable.

TABLE XVII. The Mg-Pd system.

Comparison of low temperature phases		
Composition % Mg	Experimental results[20,103]	*Ab initio* results (Fig. 12)
12.5	*two-phase region*	Ca_7Ge
20.0	*two-phase region*	$MgPd_4$-$D1_a$
25.0	*two-phase region*	$MgPd_3$-$D0_{23}$
		$D0_{22}$ ∼ 8.2 meV/atom *above* $D0_{23}$
33.3	*two-phase region*	$MgPd_2$-C37
37.5	*two-phase region*	Ga_3Pt_5
50.0	MgPd-B2/$L1_0$	$L1_0$
		B2 ∼ 1.8 meV/atom *above* $L1_0$
66.6	*two-phase region*	$NiTi_2$/C16
∼71.4	Mg_5Pd_2-$D8_{11}$	$D8_{11}$
75.0	Mg_3Pd-$D0_{18}$	$D0_{21}$
		$D0_{11}$ ∼ 7.6 meV/atom
		$D0_{18}$ ∼ 19.4 meV/atom *above* $D0_{21}$
80.0	Mg_4Pd *unknown*	*two-phase region*
		$D1_a$ ∼ 53.9 meV/atom *above tie line*
∼85.7	$Mg_{85}Pd_{14}$	***

At composition Mg_3Pd, the experimental phase $D0_{18}$ is found above the tie line, with $D0_{21}$ being the stable phase. There is one additional phase, $D0_{11}$, predicted with formation energy lower than $D0_{18}$. Entropic effects may account for the stability of $D0_{18}$ at finite temperature.

Crystallographic data were not available for the phase at composition Mg_4Pd. Furthermore, the $Mg_{85}Pd_{14}$ (cF396, 16) phase was excluded due to a large unit cell size and partial occupation of sites. *Ab initio* results are thus inconclusive from composition ∼Mg_4Pd.

13. Mg-Pt (magnesium-platinum)

The phase diagram has not been determined for the Mg-Pt system. The experimental phases at compositions $MgPt_7$ and $Mg_{85}Pt_7$ were not evaluated because the structures have not been completely determined. Nevertheless, the *ab initio*

TABLE XVIII. The Mg-Pt system.

Comparison of low temperature phases		
Composition % Mg	Experimental results[104,105]	*Ab initio* results (Fig. 13)
12.5	$MgPt_7$ *unknown*	Ca_7Ge
25.0	$MgPt_3$-$L1_2$	$L1_2$
33.3	–	Ga_2Hf ∼ 1.9 meV *above tieline*
50.0	MgPt-B20	MgPt-$L1_0$
		NiTi ∼ 23.9 meV/atom
		B2 ∼ 31.2 meV/atom
		B20 ∼ 149.2 meV/atom *above* $L1_0$
66.6	–	Mg_2Pt-C16
		$NiTi_2$ ∼ 10.7 meV/atom *above* C16
75.0	Mg_3Pt-$D0_{18}$	Mg_3Pt-$D0_{21}$
		$D0_{11}$ ∼ 12.0 meV/atom
		$D0_{18}$ ∼ 18.5 meV/atom *above* $D0_{21}$
∼85.7	$Mg_{85}Pt_{14}$	***

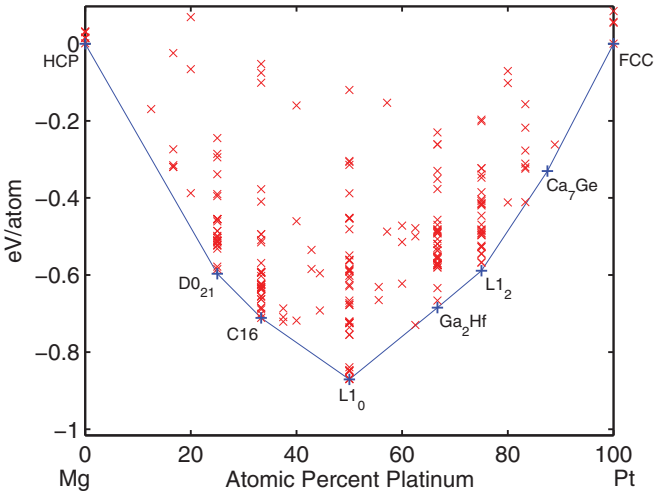

FIG. 13. (Color online) Mg-Pt convex hull.

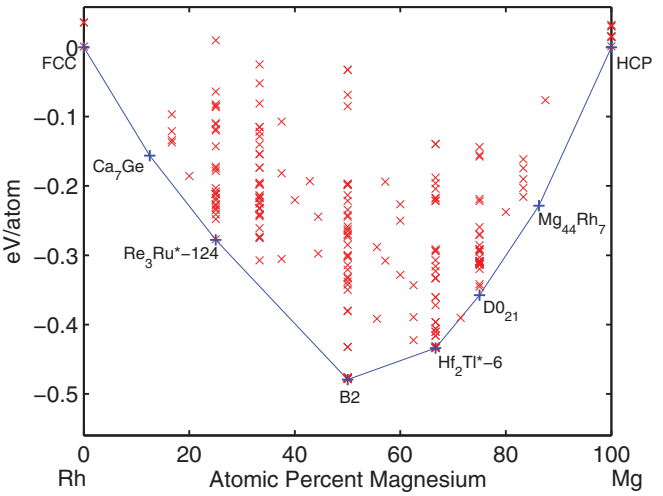

FIG. 14. (Color online) Mg-Rh convex hull.

ground state Ca_7Ge is somewhat consistent with what is known about the experimental phase at $MgPt_7$: Ca_7Ge is a doubling of the $L1_2$ structure when the 4b Wyckoff position is replaced by a Ge atom, and the experimental phase at $MgPt_7$ has been reported to consist of eight $L1_2$-type cells.[20,104]

At compositions Mg_2Pt and $MgPt_2$, phases may exist where none have been experimentally observed. While the $MgPt_2$-Ga_2Hf structure is found slightly above the tie line (∼1.9 meV), the C16 structure is stable at Mg_2Pt. We are unable to explain the surprisingly high *ab initio* energy of the MgPt-B20 phase, as well as the relative stabilities of Mg_3Pt-$D0_{21}$, -$D0_{11}$, and -$D0_{18}$, which are in contradiction to experiment. It is interesting to note, however, that an identical ordering of the phases at composition Mg_3Pt occurs in the chemically similar Mg-Pd system and that the stable *ab initio* and experimental phase at composition MgPd is $L1_0$.

14. Mg-Rh (magnesium-rhodium)

Although the phase diagram has not been determined for the Mg-Rh system, three experimental phases have been observed: MgRh-B2, Mg_5Rh_{2-x}-Al_5Co_2, and $Mg_{44}Rh_7$. The experimental phases are confirmed by *ab initio* calculations. Additional *ab initio* phases are found at compositions $MgRh_7$, $MgRh_3$, and Mg_2Rh with structures described in Table XIX.

TABLE XIX. The Mg-Rh System. A dagger (†) means see Tables II and III for crystallographic description.

Comparison of low temperature phases		
Composition % Mg	Experimental results[20]	*Ab initio* results (Fig. 14)
12.5	–	Ca_7Ge
25.0	–	Re_3Ru^*-124†
		$MgRh_3$-$D0_{22}$ ∼ 30 meV/atom *above* Re_3Ru^*-124
50.0	MgRh-B2	B2
66.6	–	Hf_2Tl^*-6†,[a]
		$NiTi_2$ ∼ 17.8 meV/atom *above* Hf_2Tl-6*
∼71.4	Mg_5Rh_2-Al_5Co_2	Al_5Co_2
75.0	–	Mg_3Rh-$D0_{21}$
∼86.3	$Mg_{44}Rh_7$	$Mg_{44}Rh_7$

[a]Tetragonal distortion of β_2[9].

15. Mg-Ru (magnesium-ruthenium)

Very little published data exist for the Mg-Ru system. The phase diagram has not been determined. Two experimental intermetallic phases are observed: Mg_3Ru_2-A13 and $Mg_{44}Rh_7$. The latter phase is not entirely determined,[20] but a rough *ab initio* evaluation of the prototype produces a thermodynamic minimum. An *ab initio* ground state is found at composition Mg_3Ru_2 with the A13 structure.

TABLE XX. The Mg-Ru system.

Comparison of low temperature phases		
Composition % Mg	Experimental results[20]	*Ab initio* results (Fig. 15)
60.0	Mg_3Ru_2-A13	A13
∼86.3	$Mg_{44}Rh_7$	$Mg_{44}Rh_7$

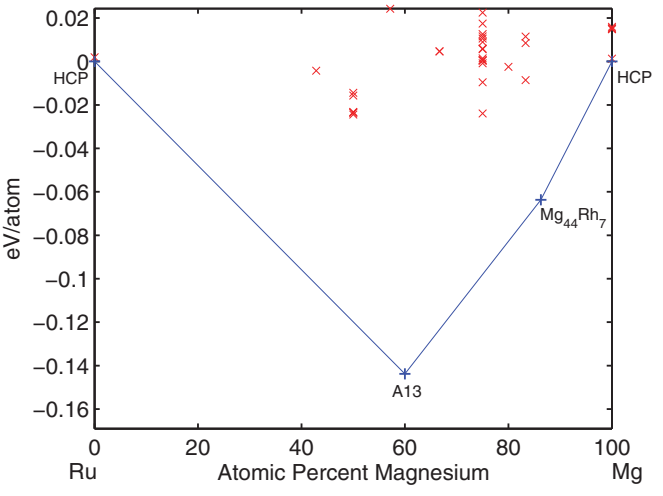

FIG. 15. (Color online) Mg-Ru convex hull.

16. Mg-Sc (magnesium-scandium)

The phase diagram for the Mg-Sc system has not been completely determined. *Ab initio* predictions of stable phases differ slightly from data reported in experimental phase diagrams. A single intermetallic compound, MgSc-B2, is reported by experiment, while three *ab initio* phases exist. The B2 phase has a slightly higher formation energy at $T = 0$ K than the *ab initio* ground state, B11. The two additional *ab initio* phases are $MgSc_2$-C49 and Mg_3Sc-$D0_{19}$.

TABLE XXI. The Mg-Sc system.

Comparison of low temperature phases		
Composition % Mg	Experimental results[20,106]	*Ab initio* results (Fig. 16)
33.3	*two-phase region*	$MgSc_2$-C49 $\beta 2$ ($FCC^{[100]}_{AB2}$) $\sim$ 3.9 meV/atom *above* C49
50.0	MgSc-B2	B11 B2 $\sim$ 5.9 meV/atom *above* B11
75.0	*two-phase region*	Mg_3Sc-$D0_{19}$ $L1_2$ $\sim$ 2.0 meV/atom *above* $D0_{19}$

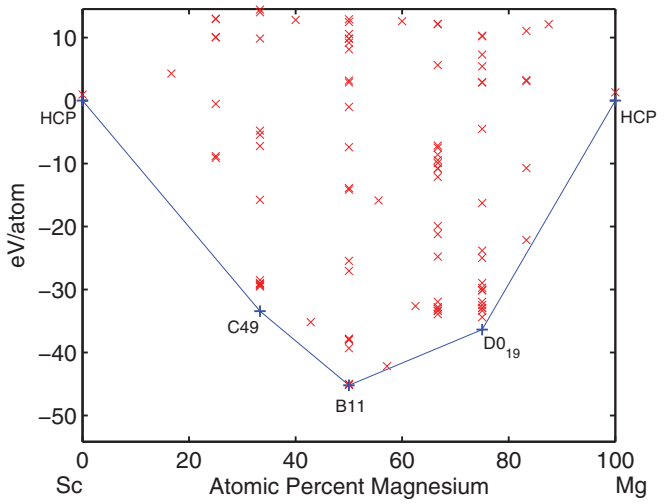

FIG. 16. (Color online) Mg-Sc convex hull.

17. Mg-Si (magnesium-silicon)

Stability of the experimental compound, Mg_2Si-C1, is corroborated by *ab initio* calculations. The clarity with which the single *ab initio* prediction arises in this system is consistent with the well-established nature of the Mg-Si system.

TABLE XXII. The Mg-Si system.

Comparison of low temperature phases		
Composition % Mg	Experimental results[20,107–113]	*Ab initio* results (Fig. 17)
66.6	Mg_2Si-C1	C1

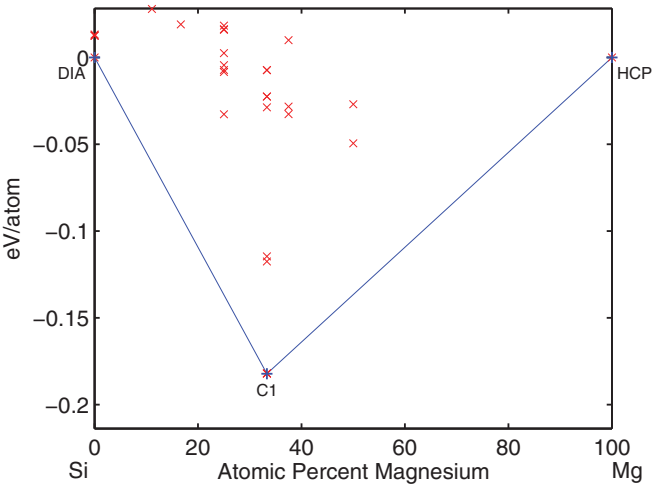

FIG. 17. (Color online) Mg-Si convex hull.

18. Mg-Sn (magnesium-tin)

A single *ab initio* ground state exists in the Mg-Sn system and occurs at the same composition and with the same structure (Mg_2Sn-C1) as the experimental compound.

TABLE XXIII. The Mg-Sn system.

Comparison of low temperature phases		
Composition % Mg	Experimental results[20,114–124]	*Ab initio* results (Fig. 18)
66.6	Mg_2Sn-C1	C1

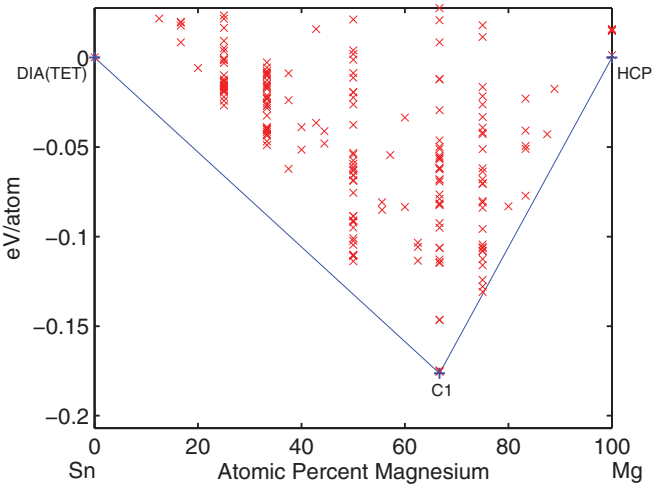

FIG. 18. (Color online) Mg-Sn convex hull.

19. Mg-Sr (magnesium-strontium)

Intermetallic compounds in the Mg-Sr system form only at Mg-rich compositions. Four experimental phases have been observed: Mg_2Sr-C14, $Mg_{23}Sr_6$-$D8_a$, $Mg_{38}Sr_9$, and $Mg_{17}Sr_2$. *Ab initio* ground states generally agree with experiment. The phase at composition $Mg_{38}Sr_9$ (hP94, 194) is described by a large unit cell above the tie line. It should be noted

TABLE XXIV. The Mg-Sr system.

Comparison of low temperature phases		
Composition % Mg	Experimental results[20,125]	*Ab initio* results (Fig. 19)
66.6	Mg_2Sr-C14	C14 C36 ∼ 1.9 meV/atom *above* C14
∼79.3	$Mn_{23}Th_6$	$Mn_{23}Th_6$
∼80.9	$Mg_{38}Sr_9$	$Mg_{38}Sr_9$ ∼ 10.4 meV/atom *above tie line*
∼89.5	$Ni_{17}Th_2$	$Ni_{17}Th_2$

also that the specification of this phase is not completely unambiguous.[20]

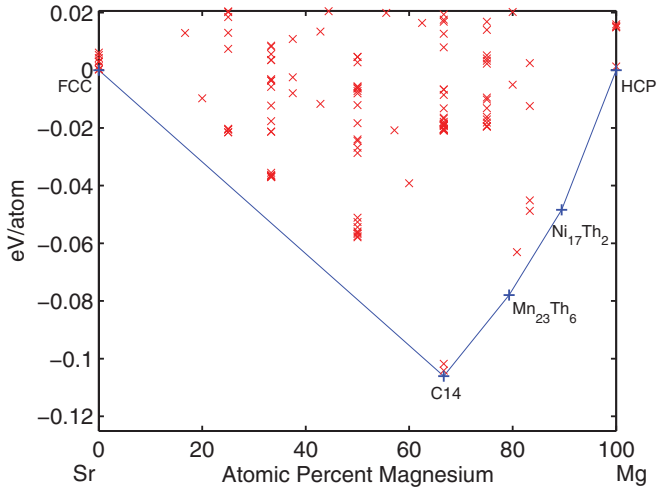

FIG. 19. (Color online) Mg-Sr convex hull.

20. Mg-Tc (magnesium-technetium)

Little published phase data exist for the Mg-Tc system, and no compounds have been reported.[20] *Ab initio* compounds are predicted: $MgTc_2$-C11$_b$, Mg_3Tc_4, and MgTc-B11.

TABLE XXV. The Mg-Tc system.

Comparison of low temperature phases		
Composition % Mg	Experimental results	*Ab initio* results (Fig. 20)
33.3	–	$MgTc_2$-C11$_b$ ∼ −15.8 meV/atom
∼42.9	–	Cu_4Ti_3 ∼ −20.2 meV/atom
50.0	–	MgTc-B11 ∼ −22.4 meV/atom

21. Mg-Y (magnesium-yttrium)

Ab initio phases are predicted in general agreement with the experimental phases found in the Mg-Y system (MgY-B2, Mg_2Y-C14, and $Mg_{24}Y_5$-A12). The Laves phase polytypes, C15, C36, and C14, are within ∼2 meV of each other and are near, although slightly above, the thermodynamic minimum

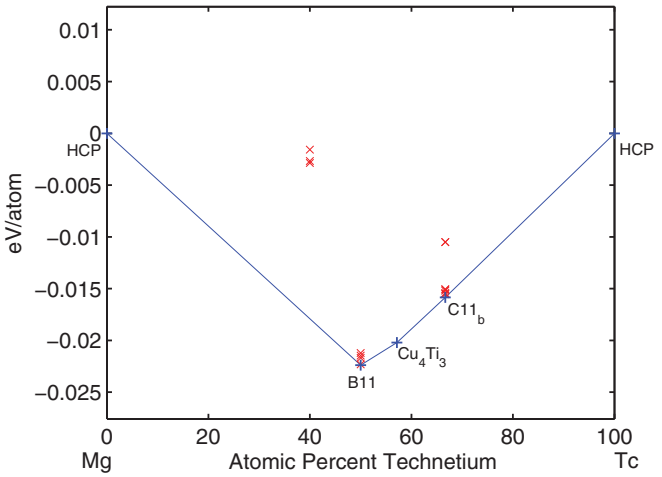

FIG. 20. (Color online) Mg-Tc convex hull.

(B2 ↔ $D0_3$). The C15 phase has the lowest formation energy and is ∼2 meV above the tie line. The $Mg_{24}Y_5$-A12 phase is similarly near, although slightly above, the thermodynamic minimum ($D0_3$ ↔ Mg-A3). However, because this "metastability" is small compared to the total energies of the system, it is reasonable to consider these as the low-temperature ground-state predictions for this system.

Additional *ab initio* phases are predicted where no experimental phases have been observed. An Y-rich phase with the C49 structure and a Mg-rich phase with the $D0_3$ structure are stable.

TABLE XXVI. The Mg-Y system.

Comparison of low temperature phases		
Composition % Mg	Experimental results[20,126–132]	*Ab initio* results (Fig. 21)
33.3	*two-phase region*	MgY_2-C49
50.0	MgY-B2	B2
66.6	Mg_2Y-C14	C15/C36/C14 ∼2 meV *above tie line*
75.0	*two-phase region*	Mg_3Y-$D0_3$ $D0_{19}$ ∼ 2.5 meV/atom *above* $D0_3$
∼82.8	$Mg_{24}Y_5$-A12	*two-phase region* A12 ∼ 3.8 meV/atom *above tie line*

22. Mg-Zn (magnesium-zinc)

The low-temperature phases of the Mg-Zn system are not completely determined. In particular, there is some ambiguity in the specification of low-temperature phases at compositions MgZn and ∼Mg_4Zn_7.

An unobserved Mg-rich phase is predicted, Mg_2Zn-C16, and there is no stable phase at composition MgZn, although the B33 structure is close to the tie line (∼8.0 meV/atom above C14 ↔ C16). The Mg_4Zn_7 phase (mS110, 12) is also thermodynamically unstable (∼11.8 meV above the tie line C14 ↔ C16). The experimental phases with structures $D8_c$

and C14 are corroborated by the existence of the same *ab initio* ground states.

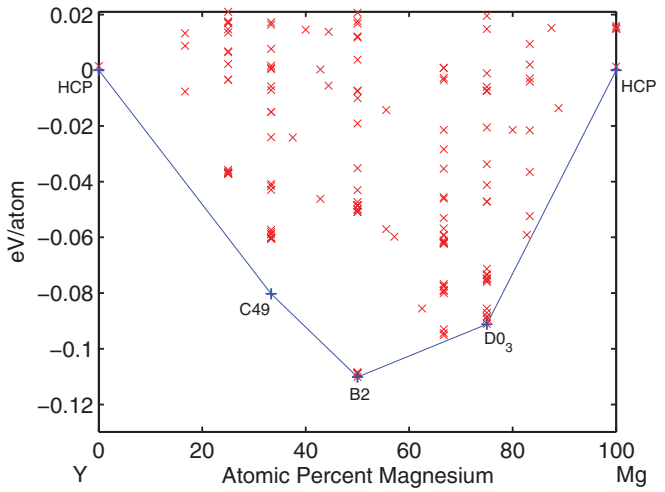

FIG. 21. (Color online) Mg-Y convex hull.

TABLE XXVII. The Mg-Zn system.

Comparison of low temperature phases		
Composition % Mg	Experimental results[20,133–144]	*Ab initio* results (Fig. 22)
∼15.3	Mg_2Zn_{11}-D8$_c$	D8$_c$
33.3	$MgZn_2$-C14	C14
∼36.3	Mg_4Zn_7	*two-phase region* Mg_4Zn_7 ∼ 11.8 meV/atom *above tie line*
50.0	MgZn *(unknown)*	*two-phase region* MgZn-B33 ∼ 8.0 meV/atom *above tie line*.
66.6	*two-phase region*	Mg_2Zn-C16

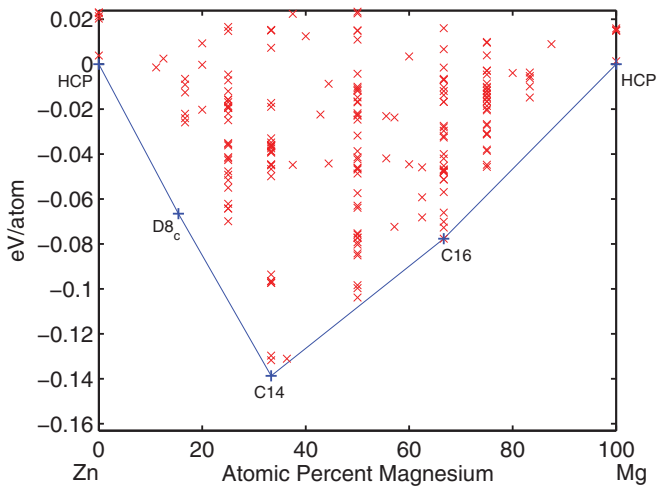

FIG. 22. (Color online) Mg-Zn convex hull.

23. Mg-Zr (magnesium-zirconium)

The Mg-Zr system has been investigated in the Mg-rich region (0 to 1 at.% Zr) with consensus regarding the existence of a peritectic reaction at ∼1 at.% Zr.[20,145–147] The existence of intermediate phases, however, has not been verified and reports of such are believed to be due to impurities.[20] Nevertheless, two stable compounds are predicted by *ab initio* calculations: Mg_3Zr_4-Cu_4Ti_3 and MgZr-B11.

TABLE XXVIII. The Mg-Zr system.

Comparison of low temperature phases		
Composition % Mg	Experimental results[20]	*Ab initio* results (Fig. 23)
∼42.9	*non-compound-forming*	Mg_3Zr_4-Cu_4Ti_3
50.0	*non-compound-forming*	MgZr-B11

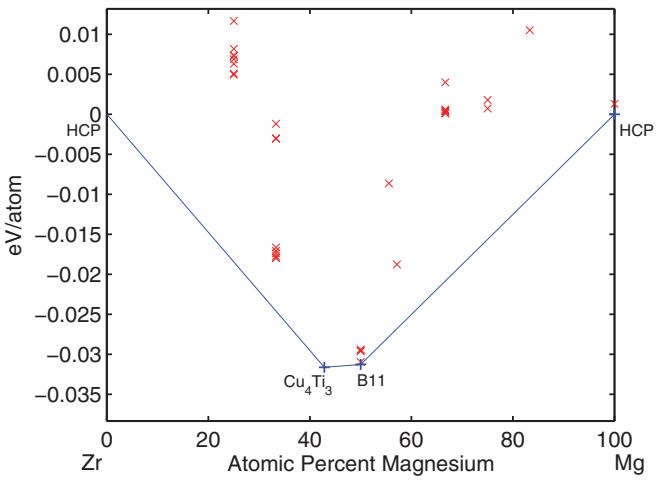

FIG. 23. (Color online) Mg-Zr convex hull.

IV. CONCLUSION

Using the AFLOW HT framework, we have explored the full composition range of 34 Mg-X binary systems at $T = 0$ K. As described in the Methods section, the accuracy of the method, η_c, can be estimated within upper and lower bounds, $86.0\% \leqslant \eta_c \leqslant 98.2\%$. In that analysis, we did not include those cases for which *ab initio* phases exist *in addition* to experimental phases. Such occurrences are frequent (found in a little more than one third of systems) and offer opportunities for alloy design. Also of interest are the non-compound-forming systems Mg-Na, Mg-Tc, and Mg-Zr with thermodynamically stable structures. These offer particularly intriguing avenues for further investigation (see Table IV).

The considerable agreement between *ab initio* predictions and experimental phases is encouraging from the standpoint of first-principles viability as a paradigm for alloy design and exploration. The first-principles methodology used here (in particular, the pseudopotential approach to atomic interactions)

is seldom pushed to the extent required by this study. Even so, the accurate prediction of experimental phases is well maintained, giving credence to *ab initio* predictions *not* corroborated by experiment.

It should be emphasized also that when *ab initio* phases contradict experiment we cannot immediately come to the conclusion of error on the part of the method. Deficiencies in the experimental characterization of binary systems exist due to the significant challenges associated with mixing alloys (e.g., impurities, kinetics). These limitations must be considered when any attempt at comparing *ab initio* ground states to experimental phases is made.

Finally, whether differences in the predictions of ground states by *ab initio* calculations are due to the limitations of first-principles methods themselves or experiment (in fact, it is unlikely to be entirely one or the other), the direction of future experiments, especially those probing difficult-to-reach regions of the binary alloy landscape, should be aided by the data presented in this work. Many avenues for further investigation are clearly presented. As examples, we mention the non-Mg-rich phases predicted in Ir-Mg, Mg-Pb, Mg-Pd, Mg-Rh, and the non-compound-forming systems with *ab initio* phases mentioned previously.

ACKNOWLEDGMENTS

We thank Wahyu Setyawan, Ohad Levy, Junkai Xue, Shidong Wang, and Mike Mehl for fruitful discussions. The research was supported by ONR (Grants. No. N00014-07-1-0878, No. N00014-07-1-1085, and No. N00014-09-1-0921) and NSF (Grants No. DMR-0639822, No. DMR-0650406, and No. DMR-0908753). We are grateful for extensive use of the Fulton Supercomputing Laboratory at Brigham Young University and Teragrid resources (MCA-07S005).

*stefano@duke.edu
†gus.hart@gmail.com

[1] G. L. W. Hart and R. W. Forcade, Phys. Rev. B **77**, 224115 (2008).
[2] EIA Energy Information Administration, *Annual Energy Review* 2009, DOE/EIA-0384 (2009).
[3] H. Zhang, S. Shang, J. Saal, A. Saengdeejing, Y. Wang, L.-Q. Chen, and Z.-K. Liu, Intermetallics **17**, 878 (2009).
[4] S. Ganeshan, S. L. Shang, H. Zhang, Y. Wang, M. Mantina, and Z.-K. Liu, Intermetallics **17**, 313 (2009).
[5] S. Curtarolo, D. Morgan, and G. Ceder, CALPHAD: Comput. Coupling Phase Diagrams Thermochem. **29**, 163 (2005).
[6] S. Curtarolo, D. Morgan, K. Persson, J. Rodgers, and G. Ceder, Phys. Rev. Lett. **91**, 135503 (2003).
[7] S. Curtarolo, W. Setyawan, G. L. W. Hart, M. Jahnatek, R. V. Chepulskii, R. H. Taylor, S. Wang, J. Xue, K. Yang, O. Levy, M. Mehl, H. T. Stokes, D. O. Demchenko, and D. Morgan, AFLOW: an automatic framework for high-throughput quantum mechanical materials discovery, (2011), [http://materials.duke.edu/aflow.html].
[8] O. Levy, G. L. W. Hart, and S. Curtarolo, J. Am. Chem. Soc. **132**, 4830 (2010).
[9] O. Levy, G. L. W. Hart, and S. Curtarolo, Acta Mater. **58**, 2887 (2010).
[10] R. H. Taylor, S. Curtarolo, and G. L. W. Hart, Phys. Rev. B **81**, 024112 (2010).
[11] R. Taylor, S. Curtarolo, and G. L. W. Hart, J. Am. Chem. Soc. **132**, 6851 (2010).
[12] O. Levy, G. L. W. Hart, and S. Curtarolo, Phys. Rev. B **81**, 174106 (2010).
[13] G. L. W. Hart and R. W. Forcade, Phys. Rev. B **80**, 014120 (2009).
[14] G. Kresse and J. Hafner, Phys. Rev. B **47**, 558 (1993).
[15] G. Kresse and D. Joubert, Phys. Rev. B **59**, 1758 (1999).
[16] J. P. Perdew, K. Burke, and M. Ernzerhof, Phys. Rev. Lett. **77**, 3865 (1996).
[17] A. N. Kolmogorov and S. Curtarolo, Phys. Rev. B **73**, 180501(R) (2006).
[18] A. N. Kolmogorov and S. Curtarolo, Phys. Rev. B **74**, 224507 (2006).
[19] P. Villars, M. Berndt, K. Brandenburg, K. Cenzual, J. Daams, F. Hulliger, T. Massalski, H. Okamoto, K. Osaki, A. Prince, H. Putz, and S. Iwata, J. Alloys Compd. **367**, 293 (2004).
[20] *Binary Alloy Phase Diagrams*, edited by T. B. Massalski, H. Okamoto, P. R. Subramanian, and L. Kacprzak (American Society for Metals, Materials Park, OH, 1990).
[21] S. Curtarolo, A. N. Kolmogorov, and F. H. Cocks, CALPHAD: Comput. Coupling Phase Diagrams Thermochem. **29**, 155 (2005).
[22] J. P. Perdew and Y. Wang, Phys. Rev. B **45**, 13244 (1992).
[23] P. Blaha, *WIEN2K An Augmented Plane Wave + Local Orbitals Program For Calculating Crystal Properties* (Vienna University of Technology, Vienna, 2001).
[24] Y. Zuo and Y. Chang, CALPHAD: Comput. Coupling Phase Diagrams Thermochem. **17**, 161 (1993).
[25] N. Saunders, CALPHAD: Comput. Coupling Phase Diagrams Thermochem. **14**, 61 (1990).
[26] E. Schürmann and R. Engel, Giessereiforschung **38**, 58 (1986).
[27] Y. Minamino, T. Yamane, T. Miyake, M. Koizumi, and Y. Miyamoto, Mater. Sci. Technol. **2**, 777 (1986).
[28] H. J. Voss and E. Schürmann, Giessereiforschung **33**, 43 (1981).
[29] E. Schürmann and I. K. Geissler, Giessereiforschung **32**, 167 (1980).
[30] M. L. Saboungi and C. C. Hsu, CALPHAD: Comput. Coupling Phase Diagrams Thermochem. **1**, 237 (1977).
[31] E. Schürmann and A. Fischer, Giessereiforschung **29**, 107 (1977).
[32] W. Wachtel, S. Woerner, and S. Steeb, Z. Metallkd. **56**, 776 (1965).
[33] K. A. Bolshakov, P. I. Fedorov, and E. I. Smarina, Russ. J. Inorg. Chem. **8**, 734 (1963).
[34] J. B. Clark and F. N. Rhines, Trans. Am. Inst. Min. Metall. Pet. Eng. **209**, 6 (1957).
[35] K. Übersicht, K. Eickhoff, and H. Vosskühler, Z. Metallkd. **44**, 223 (1953).
[36] M. I. Zakharova and V. A. Il'ina, Zh. Fiz. Khim. **24**, 714 (1950).
[37] K. Little, H. J. Axon, and W. Hume-Rothery, J. Inst. Met. **75**, 39 (1948-49).
[38] E. Butchers and W. Hume-Rothery, J. Inst. Met. **71**, 291 (1945).

[39]W. Köster and E. Wagner, Z. Metallkd. **30**, 338 (1938).
[40]W. Hume-Rothery and G. V. Raynor, J. Inst. Met. **63**, 201 (1938).
[41]W. L. Fink and L. A. Willey, Trans. Am. Inst. Min. Metall. Pet. Eng. **124**, 78 (1937).
[42]C. Goria and G. Venturello, Gazz. Chim. Ital. **67**, 487 (1937).
[43]J. L. Haughton and R. J. M. Payne, J. Inst. Met. **57**, 287 (1935).
[44]P. Saldau and M. Zamotorin, J. Inst. Met. **48**, 221 (1932).
[45]G. Siebel and E. Schmid, Z. Metallkd. **23**, 202 (1931).
[46]D. Hanson and M. L. V. Gayler, J. Inst. Met. **26**, 321 (1921).
[47]D. Hanson and M. L. V. Gayler, J. Inst. Met. **24**, 201 (1920).
[48]R. Vogel, Angew. Chem. **35**, 705 (1922).
[49]G. G. Urasow, Z. Anorg. Chem. **64**, 375 (1909).
[50]R. Vogel, Z. Anorg. Chem. **63**, 169 (1909).
[51]A. Renu, L. J. Joong, H. L. Lukas, and F. Sommer, Z. Metallkd. **86**, 103 (1995).
[52]W. Klemm and F. Dinkelacker, Z. Anorg. Chem. **255**, 2 (1947).
[53]W. Bulian and E. Fahrenhorst, Z. Metallkd. **37**, 70 (1946).
[54]H. Nowotny, E. Wormnes, and A. Mohrnheim, Z. Metallkd. **32**, 39 (1940).
[55]H. Vosskühler, Z. Metallkd. **29**, 236 (1937).
[56]J. L. Haughton, J. Inst. Met. **61**, 241 (1937).
[57]N. Baar, Z. Anorg. Chem. **70**, 352 (1911).
[58]M. Asta, R. McCormack, and D. D. de Fontaine, Phys. Rev. B **48**, 748 (1993).
[59]M. Asta, R. McCormack, and D. D. Fontaine, Giessereiforschung **36**, 53 (1984).
[60]R. Castanet, Z. Moser, and W. Gasior, CALPHAD: Comput. Coupling Phase Diagrams Thermochem. **4**, 231 (1980).
[61]G. Fischer, D. Godel, and S. Steeb, Z. Metallkd. **64**, 200 (1973).
[62]P. C. Frantz and M. Gantois, J. Appl. Crystallogr. **4**, 387 (1971).
[63]C. Frantz, M. Gantois, and A. Pianelli, C. R. Hebdomandaires Seances Acad. Sci. **265**, 1019 (1967).
[64]S. B. Felgina, Russ. Metall. Min. **6**, 96 (1964).
[65]O. Kubaschewski and T. G. Chart, J. Inst. Met. **93**, 329 (1964-65).
[66]J. B. Newkirk, Trans. Am. Inst. Min. Metall. Pet. Eng. **200**, 673 (1954).
[67]W. Hume-Rothery and G. V. Raynor, Proc. R. Soc. London **174**, 471 (1940).
[68]W. Köster and E. Wagner, Z. Metallkd. **30**, 335 (1938).
[69]E. Jünecke, Z. Metallkd. **30**, 424 (1938).
[70]G. Grube and E. Schiedt, Z. Anorg. Allg. Chem. **194**, 190 (1930).
[71]W. Hume-Rothery and S. W. Rowell, J. Inst. Met. **38**, 137 (1927).
[72]G. Bruni and C. Sandonnini, Z. Anorg. Chem. **78**, 273 (1912).
[73]G. Grube, Z. Anorg. Chem. **49**, 72 (1906).
[74]Y. Zuo and Y. A. Chang, Z. Metallkd. **84**, 662 (1993).
[75]C. A. Coughanowr, I. Ansara, R. Luoma, M. Hamalainen, and H. L. Lukas, Z. Metallkd. **82**, 574 (1991).
[76]P. Bagnoud and P. Feschotte, Z. Metallkd. **69**, 114 (1978).
[77]W. R. D. Jones, J. Inst. Met. **46**, 395 (1931).
[78]O. Dahl, Wiss. Veroeff. Siemens Werken **6**, 222 (1927).
[79]Y. K. Rao and G. R. Belton, Metall. Trans. **2**, 2215 (1971).
[80]R. Geffken and E. Miller, Trans. Metall. Soc. AIME **242**, 2323 (1968).
[81]H. Westlinning and W. Klemm, Z. Anorg. Allg. Chem. **245**, 365 (1941).
[82]G. V. Raynor, J. Inst. Met. **66**, 403 (1940).
[83]F. A. Calvo and M. P. Hierro, Rev. Metal. (Madrid, Spain) **23**, 333 (1987).
[84]W. Klemm, Angewandte Chemie **62**, 133 (1950).
[85]H. Nowotny, Z. Metallkd. **37**, 130 (1946).
[86]L. B. Hunt, Platinum Met. Rev. **31**, 32 (1987).
[87]R. Ferro, G. Rambaldi, and R. Capelli, J. Less Common Met. **4**, 16 (1962).
[88]M. Giovannini, A. Saccone, R. Marazza, and R. Ferro, Metall. Trans. A **26**, 5 (1995).
[89]P. Manfrinetti and K. J. Gschneidner, J. Less Common Met. **123**, 267 (1986).
[90]R. Joseph and K. J. Gschneidner, Trans. Metall. Soc. AIME **233**, 2063 (1965).
[91]S. Felgina, Russ. Metall. Min. **6**, 96 (1964).
[92]R. Vogel and T. Heumann, Z. Metallkd. **38**, 1 (1947).
[93]F. Weibke and W. Schmidt, Z. Elektrochem. Angew. Phys. Chem. **46**, 357 (1940).
[94]H. Abe, K. Ito, and T. Suzuki, Acta Metall. **18**, 991 (1970).
[95]C. D. G. Graham Jr., J. A. Burgo, J. W. Cooper, C. L. Douglas, P. S. Gilman, W. T. Kelley, and A. Nagelberg, Metall. Trans. **2**, 2964 (1971).
[96]J. M. Eldridge, E. Miller, and K. L. Komarek, Trans. Metall. Soc. AIME **233**, 1303 (1965).
[97]G. W. Horsley and J. T. Maskrey, J. Inst. Met. **86**, 446 (1957-1958).
[98]F. Foote and E. R. Jette, Transactions of the American Institute of Mining, Metallurgical and Petroleum Engineers **143**, 124 (1941).
[99]G. V. Raynor, J. Inst. Met. **66**, 403 (1940).
[100]H. Vosskühler, Z. Metallkd. **31**, 109 (1939).
[101]J. Goebel, Z. Metallkd. **14**, 357 (1922).
[102]N. S. Kurnakow and N. J. Stepanow, Z. Anorg. Chem. **46**, 177 (1905).
[103]E. M. Savitskii, V. F. Terekhova, and N. A. Birun, Russ. J. Inorg. Chem. **7**, 1228 (1962).
[104]W. Bronger and W. Klemm, Z. Anorg. Allg. Chem. **319**, 58 (1962).
[105]A. A. N. Hashemi and J. B. Clark, Bull. Alloy Phase Diagrams **6**, 534 (1985).
[106]B. J. Beaudry and A. H. Daane, J. Less Common Met. **18**, 305 (1969).
[107]D. Lüdecke, Z. Metallkd. **77**, 278 (1986).
[108]P. Dörner, H. Kreig, H. L. Lukas, R. Müller, and G. Petzow, CALPHAD: Comput. Coupling Phase Diagrams Thermochem. **5**, 41 (1981).
[109]E. Schürmann and A. Fischer, Giessereiforschung **29**, 111 (1977).
[110]R. Geffken and E. Miller, Trans. Metall. Soc. AIME **242**, 2323 (1968).
[111]G. V. Raynor, J. Inst. Met. **66**, 403 (1940).
[112]B. E. H. Sawamoto, Trans. Min. Metall. Assoc. Kyoto **8**, 713 (1935).
[113]R. Vogel, Z. Anorg. Chem. **61**, 46 (1909).
[114]S. Srinivasan, Z. Metallkd. **82**, 841 (1991).
[115]B. Jönsson and J. Ågren, Metall. Trans. A **17**, 607 (1986).
[116]L. M. Pavlova and K. B. Poyarkov, Russ. J. Phys. Chem. **56**, 183 (1982).
[117]A. K. Nayak and W. Oelsen, Trans. Indian Inst. Met. **21**, 15 (1968).
[118]J. M. Eldridge, E. Miller, and K. L. Komarek, Trans. Metall. Soc. AIME **236**, 114 (1966).
[119]S. B. Felgina, Russ. Metall. Min. **6**, 96 (1964).
[120]M. Wobst, Z. Phys. Chem., Abt. B **219**, 239 (1962).
[121]G. V. Raynor, J. Inst. Met. **66**, 403 (1940).

[122]W. Hume-Rothery, J. Inst. Met. **35**, 295 (1926).
[123]W. Hume-Rothery, Z. Anorg. Chem. **46**, 177 (1905).
[124]G. Grube, Z. Anorg. Chem. **46**, 76 (1905).
[125]W. Klemm and F. Dinkelacker, Z. Anorg. Chem. **255**, 2 (1947).
[126]Q. Ran, H. L. Lukas, G. Effenberg, and G. Petzow, CALPHAD: Comput. Coupling Phase Diagrams Thermochem. **12**, 375 (1988).
[127]Z. A. Sviderskaya and E. M. Padezhnova, Russ. Metall. **6**, 126 (1968).
[128]D. Miannay, P. Grégoire, P. Azou, and P. Bastien, C. R. Hebdomadaires Seances Acad. Sci., Ser. C **265**, 1107 (1967).
[129]J. F. Smith, D. M. Bailey, D. B. Novotny, and J. E. Davison, Acta Metall. **13**, 889 (1965).
[130]I. L. Markova, V. F. Terekhova, and E. M. Savitskii, Vopr. Teor. Primen. Redkozem. Met., Mater. Soveshch., 124 (1964).
[131]D. Mizer and J. B. Clark, Trans. Am. Inst. Min., Metall. Pet. Eng. **221**, 207 (1961).
[132]E. D. Gibson and O. N. Carlson, Trans. Am. Soc. Met. **52**, 1084 (1960).
[133]T. Gödecke and F. Sommer, Z. Metallkd. **85**, 683 (1994).
[134]R. Agarwal, S. G. Fries, H. L. Lukas, G. Petzow, F. Sommer, T. G. Chart, and G. Effenberg, Z. Metallkd. **83**, 216 (1992).
[135]M. E. Drits, Z. A. Sviderskaya, E. S. Kadaner, and S. B. Felgina, Russ. Metall. Min. **5**, 90 (1963).
[136]K. P. Adnerko, E. J. Klimek, D. W. Levinson, and W. Rostoker, Trans. Am. Soc. Met. **49**, 778 (1957).
[137]J. B. Clark and F. N. Rhines, Trans. Am. Inst. Min., Metall. Pet. Eng. **209**, 425 (1957).
[138]W. Klemm, Angew. Chem. **62**, 133 (1950).
[139]F. Laves, Naturwissenschaften **27**, 454 (1939).
[140]W. Hume-Rothery and E. O. Rounsefell, J. Inst. Met. **41**, 119 (1929).
[141]R. Chadwick, J. Inst. Met. **39**, 285 (1928).
[142]G. Bruni and C. Sandonnini, Z. Anorg. Chem. **78**, 273 (1912).
[143]I. Mitteilung, G. Bruni, C. Sandonnini, and E. Quercigh, Z. Anorg. Chem. **68**, 73 (1910).
[144]G. Grube, Z. Anorg. Chem. **49**, 72 (1906).
[145]R. Arroyave, D. Shin, and Z.-K. Liu, CALPHAD: Comput. Coupling Phase Diagrams Thermochem. **29**, 230 (2005).
[146]R. L. Crosby and K. A. Fowler U.S. Bur. Mines, Rep. Invest. No. 6078 (1962).
[147]I. M. Vesey and H. J. Bray, J. Inst. Met. **92**, 383 (1963–1964).